

Combination of UAV and terrestrial photogrammetry to assess rapid glacier evolution and map glacier hazards

Fugazza, Davide¹; Scaioni, Marco²; Corti, Manuel²; D'Agata, Carlo³; Azzoni, Roberto Sergio³; Cernuschi, Massimo⁴; Smiraglia, Claudio¹; Diolaiuti, Guglielmina Adele³

¹Department of Earth Sciences 'A.Desio', Università degli studi di Milano, 20133 Milano Italy

²Department of Architecture, Built Environment and Construction Engineering, Politecnico di Milano, 20133 Milano Italy

³Department of Environmental science and policy (DESP), Università degli studi di Milano, 20133 Milano Italy

⁴Agricola 2000 S.C.P.A., 20067 Tribiano (MI) Italy

Correspondence to: Marco Scaioni (marco.scaioni@polimi.it)

Abstract

Tourists and hikers visiting glaciers all year round face hazards such as the rapid formation of collapses at the terminus, typical of such a dynamically evolving environment. In this study, we analysed the potential of different survey techniques to analyze hazards of the Forni glacier, an important glacier located in Stelvio Park (Italian Alps). We carried out surveys in the ablation season 2016 and compared point clouds generated from UAV, close range photogrammetry and terrestrial laser scanning (TLS). To investigate the evolution of glacier hazards and evaluate the glacier thinning rate, we also used UAV data collected in 2014 and a DEM from an aerial photogrammetric survey of 2007. We found that the integration between terrestrial and UAV photogrammetry is ideal to map hazards related to the glacier collapse, while TLS is affected by occlusions and logistically complex in glacial terrain. Photogrammetric techniques can therefore replace TLS for glacier studies and UAV-based DEMs hold potential to become a standard tool to investigate the glacier geodetic mass balance. Based on our datasets, an increase in the size of collapses was found over the study period, and the glacier thinning rates went from $4.55 \pm 0.24 \text{ ma}^{-1}$ between 2007 and 2014 to $5.20 \pm 1.11 \text{ ma}^{-1}$ between 2014 and 2016.

1 Introduction

Glacier and permafrost-related hazards can be a serious threat to humans and infrastructure in high mountain regions (Carey et al., 2014). The most catastrophic cryospheric hazards are generally related to the outburst of water, either through breaching of moraine- or ice-dammed lakes or from the englacial or subglacial system, causing floods and debris flows. Ice avalanches from hanging glaciers can also have serious consequences for downstream populations (Vincent et al., 2015), as well as debris flows caused by the mobilization of accumulated loose sediment on steep slopes (Kaab et al.,

2005a). Less severe hazards, but still particularly threatening for mountaineers are the detachment of seracs (Riccardi et al., 2010) or the collapse of ice cavities (Gagliardini et al., 2011; Azzoni et al., submitted). While these processes are in part typical of glacial and periglacial environments, there is evidence that climate change is increasing the likelihood of specific hazards (Kaab et al., 2005a). In the European Alps, accelerated formation and growth of proglacial moraine-dammed lakes has been reported in Switzerland, amongst concern of possible overtopping of moraine dams provoked by ice avalanches (Gobiet et al., 2014). Ice avalanches themselves can be more frequent as basal sliding is enhanced by the abundance of meltwater in warmer summers (Clague, 2013). Glacier and permafrost retreat, which have been reported in all sectors of the Alps (Smiraglia et al., 2015; Fischer et al., 2014; Gardent et al., 2014; Harris et al., 2009), are a major cause of slope instabilities which can result in debris flows, by debutting rock and debris flanks and promoting the exposure of unconsolidated and ice-cored sediments (Keiler et al., 2010; Chiarle et al., 2007). Glacier downwasting is also increasing the occurrence of structural collapse and while not directly threatening human lives, sustained negative glacier mass balance can also cause shortages of water for industrial, agricultural and domestic use and energy production, affecting even populations living away from glaciers. Finally, glacier retreat and the increase in glacier hazards negatively influence the tourism sector and the economic prosperity of high mountain regions (Palomo, 2017).

The increasing threat from cryospheric hazards under climate change calls for the adoption of mitigation strategies. Remote Sensing has long been recognized as an important tool to produce supporting data to this purpose, owing to the ability to generate digital elevation models (DEMs) and multispectral images. DEMs are particularly useful to detect glacier thickness and volume variations (Fischer et al., 2015; Berthier et al., 2016) and to identify steep areas that are most prone to geomorphodynamic changes such as mass movements (Blasone et al., 2014). Multispectral images at a

55 sufficient spatial resolution enable the recognition of most cryospheric hazards (Quincey et al, 2005;
56 Kaab et al., 2005b). While satellite images from Landsat and ASTER sensors (15-30 m ground sample
57 distance - GSD) are practical for regional-scale mapping (Rounce et al, 2017), the assessment of
58 hazards at the scale of individual glaciers or basins requires higher spatial resolution, which in the past
59 could only be achieved via dedicated field campaigns with terrestrial laser scanners (TLS) (Krenner-
60 Pirklbauer et al., 2005; Riccardi et al., 2010). Recent years have seen a resurgence of terrestrial
61 photogrammetric surveys for the generation of DEMs (Piermattei et al., 2015, 2016; Kaufmann and
62 Seier, 2016) due to important technological advancements including the development of Structure-
63 from-Motion (SfM) Photogrammetry and its implementation in fully automatic processing software, as
64 well as the improvements in the quality of camera sensors (Eltner et al., 2016; Westoby et al., 2012). In
65 parallel, unmanned aerial vehicles (UAVs – Colomina & Molina, 2014, O'Connor et al., 2017) have
66 started to emerge as a viable alternative to TLS for multi-temporal monitoring of small areas. UAVs
67 promise to bridge the gap between field observations, notoriously difficult on glaciers, and coarser
68 resolution satellite data (Bhardwaj et al., 2016). Although the number of studies employing them in
69 high mountain environments is slowly increasing (see e.g. Fugazza et al., 2015; Gindraux et al., 2017;
70 Seier et al, 2017), their full potential for monitoring of glaciers and particularly glacier hazards has still
71 to be explored. In particular, the advantages of UAV and terrestrial SfM-Photogrammetry, and the
72 possibility of data fusion to support hazard management strategies in glacial environments needs to be
73 investigated and assessed.

74 In this study, we investigated a rapidly downwasting glacier in a protected area and highly touristic
75 sector of the Italian Alps, Stelvio National Park. We focused on the glacier terminus and the hazards
76 identified there, i.e., the formation of normal faults and ring faults. The former occur mainly on the
77 medial moraines and glacier terminus and are due to gravitational collapse of debris-laden slopes. The latter

78 develop as a series of circular or semicircular fractures with stepwise subsidence, caused by englacial or
79 subglacial meltwater creating voids at the ice-bedrock interface and eventually the collapse of cavity roofs.
80 While often overlooked, these collapse structures are particularly hazardous for mountaineers and likely to
81 increase under a climate change scenario (Azzoni et al., submitted). They are more dangerous than
82 crevasses because of their larger size and because they could be filled with snow and rendered entirely or
83 partly invisible to mountaineers.

84 We conducted our first UAV survey of the glacier in 2014; then, through a dedicated field campaign
85 carried out in summer 2016, we compared different platforms and techniques for point cloud, DEM and
86 orthomosaic generation to assess their ability to monitor glacier hazards: UAV photogrammetry,
87 terrestrial photogrammetry and TLS. The aims were: (1) comparing UAV- and terrestrial
88 photogrammetric products acquired in 2016 against the TLS point cloud; (2) identifying glacier-related
89 hazards and their evolution between 2014-2016 using the merged point cloud from UAV and terrestrial
90 photogrammetry and UAV orthophotos; and 3) investigating ice thickness changes between 2014-2016
91 and 2007-2016 by comparing the two UAV DEMs and a third DEM obtained from stereo-processing of
92 aerial photos captured in 2007.

93

94 2 Study Area

95 The Forni Glacier (see Fig. 1) has an area of 11.34 km² based on the 2007 data from the Italian Glacier
96 Inventory (Smiraglia et al., 2015), an altitudinal range between 2501 and 3673 m a.s.l. and a North-
97 North-Westerly aspect. The glacier retreated markedly since the little ice age (LIA), when its area was
98 17.80 km² (Diolaiuti & Smiraglia, 2010), with an acceleration of the shrinking rate in the last three
99 decades, typical of valley glaciers in the Alps (Diolaiuti et al., 2012, D'Agata et al.; 2014). It has also
100 undergone profound changes in dynamics in recent years, including the loss of ice flow from the
101 eastern accumulation basin towards its tongue and the evidence of collapsing areas on the eastern



102 tongue (Azzoni et al., submitted). One such area, hosting a large ring fault (see Fig. 2d) prompted an
103 investigation carried out with Ground Penetrating Radar (GPR) in October 2015, but little evidence of
104 a meltwater pocket was found under the ice surface (Fioletti et al., 2016). Since then, a new ring fault
105 appeared on the central tongue, and the terminus underwent substantial collapse (see Fig. 2a,b,c,e).
106 Continuous monitoring of these hazards is important as the site is highly touristic (Garavaglia et al.,
107 2012), owing to its location in Stelvio Park, one of Italy's major protected areas, and its inclusion in the
108 list of geosites of Lombardy region (see Diolaiuti and Smiraglia, 2010). The glacier is in fact frequently
109 visited during both summer and winter months. During the summer, hikers heading to Mount San
110 Matteo take the trail along the central tongue, accessing the glacier through the left flank of the
111 collapsing glacier terminus. During wintertime, ski-mountaineers instead access the glacier from the
112 eastern side, crossing the medial moraine and potentially collapsed areas there (see Fig. 1).



113 **3 Data Sources: acquisition and processing**

114 **3.1 UAV Photogrammetry**

115 **3.1.1 2014 Dataset**

116 The first UAV survey took place on 28th August 2014, using a SwingletCam fixed wing aircraft (see
117 Fig. 3a). This commercial platform developed by SenseFly carries a Canon Ixus 127 HS compact
118 digital camera. The UAV was flown in autopilot mode with a relative flying height of approximately
119 380 m above the glacier surface, which resulted in an average GSD of 12 cm. The flight plan was
120 organized by using the proprietary software eMotion, by which the aircraft follows predefined
121 waypoints with a nominal along-strip overlap of 70%; sidelap was not regular because of the varying
122 surface topography, but was approximately 60%. Flight operations started at 07:22 AM and ended at
123 08:22 AM. Early morning operations were preferred to avoid saturating camera pictures, as during this
124 time of day the glacier is not yet directly illuminated by the sun, and to minimize blurring effects due to



125 the UAV motion, since wind speed is at its lowest on glaciers during morning hours (Fugazza et al.,
126 2015). Pictures were automatically captured by the UAV platform, selecting the best combination of
127 sensor aperture ($F=2.7$), sensitivity (between 100-400 ISO) and shutter speed (between 1/125 s - 1/640
128 s). The survey covered an area of 2.21 km² in just two flight campaigns, with a low altitude take-off
129 (lake Rosole, close to Branca Hut, see Fig. 1). Both the terminal parts of the central and eastern
130 ablation tongue were surveyed.

131 Processing of data from the 2014 UAV flight was carried out using Agisoft Photoscan version 1.2.4
132 (www.agisoft.com), implementing a SfM algorithm for image orientation (Spetsakis and Armonos,
133 1991) followed by a multi-view dense-matching approach for surface 3D reconstruction (Furukawa and
134 Ponce, 2009). Since no GCPs were measured during the 2014 campaign, the registration of this data set
135 into the mapping reference system was based on GNSS (Global Navigation Satellite System)
136 navigation data only. Consequently, a global bias in the order of 1.5-2 m resulted after geo-referencing,
137 and no control on the intrinsic geometric block stability could be possible. After the generation of the
138 point cloud, a DEM and orthoimage were produced using the method described by Immerzeel et al.
139 (2014), with spatial resolutions of 60 cm and 15 cm, respectively.

140

141 3.1.2 2016 Dataset

142 The UAV surveys were carried out on 30th August and 1st September 2016, both around midday
143 with 8/8 of the sky covered by stratocumulus clouds. The UAV employed in these surveys was a
144 customized quadcopter (see Fig. 3b) carrying a Canon Powershot 16 Megapixel digital camera. Two
145 different take-off and landing sites were chosen to gain altitude before take-off and maintain line-of-
146 sight operation with a flying altitude of 50 m above ground, which ensured an average ground sample
147 distance (GSD) of 6 cm. The first take-off site was on the eastern lateral moraine (elevation approx.



148 2700 m a.s.l.), while the second site was a rock outcrop on the hydrographic left flank of the glacier
149 (see Fig. 1) at an elevation of approx. 2750 m a.s.l. To reduce motion blur, camera shutter speed was
150 set to the lowest possible setting, 1/2000 s, with aperture at F/2.7 and sensitivity at 200 ISO.



151 Several individual parallel flights were conducted to cover a small section of the proglacial plain and
152 different surface types on the glacier surface, including the terminus, a collapsed area on the central
153 tongue, the eastern medial moraine and some debris-covered parts of the eastern tongue. A 'zig-zag'
154 flying scheme was followed to reduce the flight time. The UAV was flown in autopilot mode using the
155 open-source software Mission Planner (Oborne, 2013) to ensure 70% along-strip overlap and sidelap.
156 In total, two flights were performed during the first survey and three during the second, lasting about
157 20 minutes each. The surveyed area spanned over 0.59 km².



158 Processing of data from the 2016 UAV flight was carried out using Agisoft Photoscan vers 1.2.4.
159 Eight GCPs (see Fig. 1) were measured for the registration of the photogrammetric blocks and its by-
160 products into the mapping system. The root mean square error (RMSE) of the GCPs was 40 cm, which
161 can be used as an indicator of accuracy for the geo-referencing of the photogrammetric block. The
162 point cloud obtained from the 2016 UAV flight was interpolated to produce a DEM and orthoimage
163 with the same cell resolution as the 2014 dataset, i.e., 60 and 15 cm, respectively. Both products were
164 exported in the ITRS2000 / UTM 32N mapping reference system.

165 3.2 Terrestrial photogrammetry

166 The terrestrial photogrammetric survey was carried out during on 29th August 2016 to reconstruct the
167 topographic surface of the glacier terminus, which presented several vertical and subvertical surfaces
168 whose measurement was not possible from the UAV platform carrying a camera in nadir configuration
169 (see Fig. 2e).



170 Images were captured from 134 ground-based stations, most of them located in front of the glacier, and
171 some on both flanks of the valley in the downstream area, as shown in Fig. 4a. A single-lens-reflex
172 Nikon D700 camera was used, equipped with a 50 mm lens, and a full-frame CMOS sensor (36x24
173 mm) with 4256x2823 pixels. This photogrammetric block was processed using Agisoft Photoscan
174 version 1.2.4. In this case, since no preliminary information about approximate camera position was
175 collected, the SfM procedure was run without any initial information.

176 Seven natural features visible on the glacier front were used as GCPs to be included in the bundle
177 adjustment computation in Agisoft Photoscan. Measurement of GCPs in the field was carried out by
178 means of a high-precision theodolite. The measurement of points previously recorded with a GNSS
179 geodetic receiver allowed to register the coordinates of GCPs in the mapping reference system. The
180 RMSE of 3D residual vectors on GCPs was 34 cm, which can be considered as the accuracy of
181 absolute geo-referencing. The final point cloud obtained from the dense matching tool implemented in
182 Agisoft Photoscan covers at a very high spatial resolution the full glacier terminus, with the exception
183 of a few obstructed parts (see Fig. 4b).

184 3.3 Terrestrial Laser Scanning

185 On the same days as the first UAV survey of 2016, a long-range terrestrial laser scanner Riegl LMS-
186 Z420i was used to scan the glacier terminus frontally. One instrumental standpoint located on the
187 hydrographic left flank of the glacier terminus (see Fig. 1) was established. The horizontal and vertical
188 scanning resolution were set up to provide a spatial point density of approx. 5 cm on the ice surface at
189 the terminus. Geo-referencing was accomplished by placing five GCPs consisting in cylinders covered
190 by retroreflective paper. The coordinates of GCPs were measured by using a precision theodolite
191 following the same procedure adopted for terrestrial photogrammetry. Considering the accuracy of

192 registration and the expected precision of laser point measurement, the global accuracy of 3D points
193 was estimated in the order of ± 7.5 cm.

194 3.4 GNSS ground control points

195 Prior to the 2016 surveys, eight control targets were placed both outside the glacier and on the glacier
196 tongue (see Fig. 1). Differential GNSS data were acquired at their location for accurate geo-referencing
197 of UAV, terrestrial photogrammetry and TLS data. While for geo-referencing of UAV data the GCPs
198 were directly visible on the quadcopter images, for terrestrial photogrammetry and TLS they were
199 adopted for the registration of theodolite measurements. The targets consisted in a piece of white fabric
200 80 x 80 cm wide, with a circular marker in red paint chosen to provide contrast against the background.
201 Except for the one GCP located at the highest site, such GCPs were positioned on large, flat boulders to
202 provide a stable support and reduce the impact of ice ablation between flights.

203 GNSS data were acquired by means of a pair of Leica Geosystems 1200 geodetic receivers working in
204 RTK (Real-Time Kinematics) mode (see Hoffman-Wellenhof, 2008). One of them was set up as master
205 on a boulder beside Branca Hut, where a monument had been established with known coordinates in
206 the mapping reference system ITRS2000 / UTM 32N. The second receiver was used as a rover,
207 communicating via radio link with the master station. The maximum distance between master and
208 rover was less than 1.5 km, but the local topography prevented broadcasting the differential corrections
209 in a few zones of the glacier. Unfortunately, no mobile phone services were available and consequently
210 the internet network could not be accessed, precluding the use of the regional GNSS real-time
211 positioning service. Non-RTK points were processed in fast-static mode, requiring a longer
212 measurement time of approx. 12 minutes. The theoretical accuracy of GCPs was estimated in the order
213 of 2-3 cm.

214 3.5 2007 DEM

215 The 2007 TerraItaly DEM was produced by BLOM C.G.R. company for Lombardy region. It is the
216 final product of an aerial survey over the entire region, that was conducted with a multispectral
217 pushbroom Leica ADS40 sensor acquiring images from a flying height of 6,300 m with an average
218 GSD of 65 cm. The images were processed to generate a DEM with a cell resolution of 2 m x 2 m, and
219 projected in the former national ‘Gauss Boaga - Fuso I’ mapping reference system based on Monte
220 Mario datum (Mugnier, 2005). Heights were converted from ellipsoidal to geodetic using the official
221 software for datum transformation in Italy (Verto ver. 3), which is distributed by the Italian Geographic
222 Military Institute (IGMI). The final vertical accuracy reported by BLOM C.G.R. is ± 3 m. The only
223 processing step performed within this study was the datum conversion to ITRS2000, using a seven
224 parameter similarity transformation based on a local parameter set provided by IGMI.



225 4 Methods

226 4.1 Analysis of point clouds from the 2016 campaign: UAV/terrestrial photogrammetry and TLS

227 The comparison between point clouds generated during the 2016 campaign had the aim of assessing
228 their geometric quality before their application for the analysis of hazards. These evaluations were also
229 expected to provide some guidelines for the organization of future investigations in the field at the
230 Forni Glacier and in other Alpine sites. Specifically, we analysed point density (points/m²) and
231 completeness, i.e. % of area in the ray view angle. Point density partly depends upon the adopted
232 surveying technique, since it is controlled by the distance between sensor and surface and the
233 obtainable spatial resolution. In SfM-Photogrammetry, the latter property is affected by dense
234 matching, while in TLS it can be set up as data acquisition input parameter. In this study, the number of
235 neighbours N (inside a sphere of radius $R=1$ meter) divided by the neighbourhood surface was used to
236 evaluate the local point density D in CloudCompare (www.cloudcompare.org). To understand the

237 effect of point density dispersion (Teunissen, 2009), the inferior 12.5 percentile of the standard
238 deviation σ of point density was also calculated. The use of these local metrics allowed to distinguish
239 between point density in different areas, since this may largely change from one portion of surface to
240 another. A further metric in this sense was point cloud completeness, referring to the presence of
241 enough points to completely describe a portion of surface. In this study, the visual inspection of
242 selected sample locations was used to identify occlusions and areas with lower point density.

243 To analyse these properties, five regions were selected (see Fig. 5), located on the glacier topographic
244 surface and characterized by different glacier features and the presence of hazards: 1) Glacial cavity
245 composed by subvertical and fractured surfaces over 20 m high, and forming a typical semicircular
246 shape; 2) glacial cavity over 10 m high with the same typical semi-circular shape as location 1, covered
247 by fine- and medium-size rock debris; 3) normal fault over 10 m high; 4) highly-collapsed area covered
248 by fine- and medium-size rock debris and rock boulders; and 5) planar surface with a normal fault
249 covered by fine- and medium-size rock debris and rock boulders. The analysis of local regions was
250 preferred to the analysis of the entire point clouds for the following reasons: 1) the incomplete overlap
251 between point clouds obtained from different methods; 2) the opportunity to investigate the
252 performances of the techniques in diverse geomorphological situations.







253  Finally, we compared the point clouds in a pairwise manner within the same sample locations. Since no
254 available benchmarking data set (e.g. accurate static GNSS data) was ~~concurrently~~ collected during the
255 2016 campaign, the TLS point cloud was used as a reference, as it less influenced by controlling
256  factors (network geometry, object texture, lighting conditions). When comparing both photogrammetric
257 data sets, the one obtained from UAV was used as reference because of the even distribution of point
258 density within the sample locations. The presence of residual, non-homogenous geo-referencing errors
259 in the data sets required a specific fine registration of each individual sample location, which was

260 conducted in CloudCompare using the ICP algorithm (Pomerleau et al., 2016). Then, point clouds in
261 corresponding sample areas were compared using the M3Cz algorithm implemented in CloudCompare
262 (Lague et al., 2013). This solution allowed us to get rid of registration errors from the analysis, which
263 could then be focused on the capability of the adopted techniques to reconstruct the local geometric
264 surface of the glacier in an accurate way.

265 4.2 Merging of UAV and close-range photogrammetric point clouds

266 To improve coverage of different glacier surfaces, including planar areas and normal faults,
267 photogrammetric point clouds from the 2016 campaign were merged. Prior to point cloud merging, a
268 preliminary co-registration was performed on the basis of the ICP algorithm in CloudCompare.
269 Regions common to both point clouds were used to minimize the distances between them and find the
270 best co-registration. The point cloud from UAV photogrammetry, which featured the largest extension,
271 was used as reference during co-registration, while the other was rigidly transformed to fit with it.
272 After this task, both original point clouds resulted aligned into the same reference system. In order to
273 get rid of redundant points and to obtain a homogenous point density, the merged point cloud (see Fig.
274 5) was subsampled keeping a minimum distance between adjacent points of 20 cm. The final size of
275 this data set is approximately 4.4 million points, which represents a manageable data amount on up-to-
276 date computers. The colour RGB information associated to each point in the final point cloud was
277 derived by averaging the RGB information of original points in the subsampling volumes. While this
278 operation resulted in losing part of the original RGB information, it helped provide a realistic
279 visualization of the topographic model, which can aid the interpretation of glacier hazards.



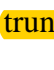


280 4.2 Glacier hazard mapping

281 The investigation of glacier hazards was conducted by considering datasets from 2014 and 2016. In
282 2014,  the point cloud and UAV orthophoto were available, while in 2016 the point cloud obtained
283 by merging UAV and  close-range photogrammetric data sets was used in combination with the UAV
284 orthophoto.  In this study, we focused on ring faults and normal faults, which were manually delineated 
285 by using geometric properties from the point clouds while color information from orthophotos was
286 used as a cross-check. ~~On point clouds, mapping is based on visual inspection of vertical displacements~~
287 ~~following faulting or subsidence.~~ On orthophotos, both types of structures also generally appear as
288 linear features in contrast with their surrounding  these structures may look similar to crevasses,
289 further information concerning their orientation and location needs to be assessed for discrimination.
290 The orientation of fault structures is not coherent with glacier flow, with ring faults also appearing in 
291 circular patterns. Their location is limited to the glacier margins, medial moraines and terminus
292 (Azzoni et al., submitted). After delineation, we also analysed the height of vertical facies using
293 information from the point clouds.

294 4.3 DEM co-registration for glacier thickness change estimation

295 Several studies have found that errors in individual DEMs, both in the horizontal and vertical domain,
296 propagate when calculating their difference leading to inaccurate estimations of thickness and volume
297 change (Berthier et al., 2007; Nuth & Kaab, 2011). In the present study, different approaches were
298 adopted for geo-referencing all the DEMs (2007, 2014, 2016) used in the analysis of the volume
299 change of the Forni Glacier tongue. To compute the relative differences between the DEMs, a
300 preliminary co-registration was therefore required. The method proposed by Berthier et al. (2007) for
301 the co-registration of two DEMs was separately applied to each DEM pair (2007-2014; 2007-2016;
302 2014-2016). Following this method, in each pair one DEM plays as reference ('master'), while the
303 other is used as 'slave' DEM to be iteratively shifted along x and y directions by fractions of pixel to

304 minimize the standard deviation of elevation differences with respect to the ‘master’ DEM. Only areas
305 assumed to be stable are considered in the calculation of the co-registration shift. The ice-covered areas
306 were excluded by overlaying the glacier outlines from D’Agata et al. (2014) for 2007 and Fugazza et
307 al. (2015) for 2014. The oldest DEM, which is also the widest in each comparison, was always set as
308 the master. To co-register the 2014 and 2016 DEMs with the 2007 DEM, both were resampled to 2 m
309 spatial resolution, whereas the comparison between 2014 and 2016 was carried out at the original
310 resolution of these data sets (60 cm).

311 All points resulting in elevation differences larger than 15 m were labelled as unreliable, and
312 consequently discarded from the subsequent analysis. Such larger discrepancies may denote errors in
313 one of the DEMs or unstable areas outside the glacier. Values exceeding this threshold, however, were
314 only found in a marginal area with low image overlap in the comparison between the 2014 and 2016
315 DEMs, with a maximum elevation difference of 36 m. Once the final co-registration shifts were
316 computed (see Table 1), the coefficients were subtracted from the top left coordinates of the ‘slave’
317 DEM; the residual mean elevation difference was also subtracted from the ‘slave’ DEM to bring the
318 mean to zero. After DEM co-registration, the resulting shifts reported in Table 1 were applied to each
319 ‘slave’ DEM, including the entire glacier area. Then the elevations of the ‘slave’ DEM were subtracted
320 from the corresponding elevations of the ‘master’ DEM to obtain the so called DEM of Differences
321 (DoD). Over a reference area  common to all three DEMs (Fig. 1), we estimated the volume change 
322 its uncertainty following the method proposed in Howat et al. (2008), which expresses the uncertainty
323 of volume change as the combination of the standard deviation computed from the residual elevation
324 difference over stable areas, and the  truncation error implicit when substituting the integral in volume 
325 calculation with a finite sum, according to Jokinen and Geist (2010). 

326 5 Results



327 5.1 Point cloud Analysis

328 The analysis of point density shows significant differences between the three techniques for point cloud
329 generation (see Table 2). Values range from 103 to 2297 points/m² depending on the surveying
330 method, but the density was generally sufficient for the reconstruction of the different surfaces shown
331 in Fig. 5, except for location 5. Terrestrial photogrammetry featured the highest point density, while
332 UAV photogrammetry had the lowest. In relation to UAV photogrammetry, similar point densities
333 were found in all sample locations, especially for the standard deviations that were always in the range
334 22-29 points/m². Mean values were between 103-109 points/m² in locations 2-4, while they were higher
335 in location 5 (141 points/m²). Due to the nadir acquisition points, the 3D modelling of vertical/sub-
336 vertical cliffs in location 1 was not possible. In relation to TLS, a mean value of point density ranging
337 from 141-391 points/m² was found, with the only exception of location 5, where no sufficient data were
338 recorded due to the position of this region with respect to the instrumental standpoint. Standard
339 deviations ranged between 69-217 points/m², moderately correlated with respective mean values. The
340 analysis of the completeness of surface reconstruction also revealed some issues related to the adopted
341 techniques (see Fig. 6). Specifically, TLS suffered from severe occlusions which prevented acquisition
342 of data in the central part of the sample area, while UAV photogrammetry was able to reconstruct the
343 upper portion of the sample area but not the vertical cliff. Only terrestrial photogrammetry acquired a
344 large number of points in all areas.

345 In terms of point cloud distance (see Table 3), the comparison between TLS and terrestrial
346 photogrammetry resulted in a high similarity between point clouds, with no large differences between
347 different sample areas. Conversely, the comparison between TLS and UAV photogrammetry and
348 terrestrial and UAV photogrammetry provided significantly worse results, which may be summarized
349 by the RMSEs in the range 21.1-37.7 cm and 20.7-30.4 cm, respectively. The worse values were both

350 obtained in the analysis of location 2, which mostly represents a vertical surface, while the best
351 agreement was found within location 3 which is less inclined. As the UAV flight was geo-referenced
352 on a set of GCPs with an RMSE of 40.5 cm, the ICP co-registration may have not totally compensated
353 the existing bias.

354 **5.2 Glacier-related hazards and risks**

355 The tongue of Forni glacier hosts a variety of hazardous structures. While most collapsed areas are
356 normal faults, two large ring fault systems can be identified: the first, located in the eastern section (see
357 Fig. 2d and  covered an area of $25.6 \times 10^3 \text{ m}^2$ and showed surface lowering up to 5 m in 2014. This
358 area was not surveyed in 2016, since field observation did not show evidence of further subsidence.
359 Conversely, the ring fault that only emerged as a few semi-circular fractures in 2014 grew until cavity
360 collapse, with a vertical displacement up to 20 m and further fractures extending south-eastward (see
361 Fig. 2c and  thus potentially widening the extent of collapse in the future. Further smaller ring faults
362 were identified in 2014 at the eastern glacier margin. Only one of them was included in the area
363 surveyed in 2016, with further 2 m subsidence and an increase in subparallel fractures.

364 Normal faults are mostly found on the eastern medial moraine and at the terminus. Between 2014 and
365 2016, the first developed rapidly in the vertical domain reaching a height of 12 m in 2016. The collapse
366 was even more rapid at the terminus, leading to the formation of three sub-vertical facies, up to 24 m
367 high, while the height of the vault is as low as 10 m. Several fractures also appear in conjunction with
368 the large ring fault located in the central section of the glacier, extending the fracture system to the
369 western glacier margin. It is likely that the terminus will recede along the fault system on the eastern
370 medial moraine and following the ring faults at the eastern and western margins, increasing the
371 occurrence of hazardous phenomena in these areas.

372 5.3 Glacier Thickness change

373 The Forni Glacier tongue was affected by substantial thinning throughout the observation period.
374 Between 2007 and 2014, the largest thinning occurred in the eastern section of the glacier tongue, with
375 changes persistently below -30 m whereas the upper part of the central tongue only thinned by 10/
376 m. The greatest ice loss occurred in correspondence with the normal faults localized in small areas at
377 the eastern glacier margin (see Fig. 8a), with local changes generally below -50 m and a minimum of -
378 66.80 m, owing to the formation of a lake. Conversely, between 2014 and 2016 the central and eastern
379 parts of the tongue had similar thinning patterns, with average changes of -10 m. The greatest losses are
380 mainly found in correspondence with normal faults, with a maximum change of -38.71 m at the
381 terminus and local thinning above 25 m on the lower medial moraine. The ring fault at the left margin
382 of the central section of the tongue also shows thinning of 20/26 m. In the absence of faults, little
383 thinning occurred instead on the upper part of the medial moraine, where a thick debris cover shielded
384 ice from ablation, with changes of -2/-5 m (see Fig. 8c). Considering a common reference area (see
385 Fig. 1, table 4), an acceleration of glacier thinning seems to have occurred over recent years over the
386 lower glacier tongue, from $-4.55 \pm 0.24 \text{ ma}^{-1}$ in 2007-2014 to $-5.20 \pm 1.11 \text{ ma}^{-1}$ in 2014-2016, also
387 confirmed by the value of $-4.76 \pm 0.29 \text{ ma}^{-1}$ obtained from the comparison between 2007 and 2016.
388 Looking at the first two DoD, the trend seems to be caused by the increase in collapsing areas
389 (Fig.8a,b).

390

391 6 Discussion

392 The choice of a technique to monitor glacier hazards and the glacier geodetic mass balance can depend
393 on several factors, including the size of the area, the desired spatial resolution and accuracy, logistics
394 and cost. In this study, we focused on spatial metrics, i.e. point density, completeness and distance

395 between point clouds to evaluate the performance of UAV, close-range photogrammetry and TLS in a
396 variety of conditions.

397 Considering point density, terrestrial photogrammetry resulted in a denser data set than the other
398 techniques. This is mostly motivated by the possibility to acquire data from several stations with this
399 methodology, only depending on the terrain accessibility, reducing the effect of occlusions with a
400 consequently more complete 3D modelling. However, the mean point density achieved when using
401 terrestrial photogrammetry has a large variability both between different sample locations, and inside
402 each location as shown by the standard deviations of D . Point densities related to UAV
403 photogrammetry and TLS are more regular and constant. In the case of UAV photogrammetry, the
404 homogeneity of point density is due to the regular structure of the airborne photogrammetric block. In
405 the case of TLS, the regularity is motivated by the constant angular resolution adopted during scanning.
406 Since any techniques may perform better when the surface to survey is approximately orthogonal to the
407 sensor looking direction, terrestrial photogrammetry is more efficient for reconstructing vertical and
408 subvertical cliffs (Sample areas 1 and 2) and high-sloped surfaces (Sample areas 3 and 4). On the
409 contrary, airborne UAV photogrammetry provided the best results in location 5 which is less inclined
410 and consequently could be well depicted in vertical photos. In general, point clouds from terrestrial
411 photogrammetry provide a better description of the vertical and subvertical parts (see e.g. Winkler et
412 al., 2012), while point clouds obtained from UAV photogrammetry are more suitable to describe the
413 horizontal or sub-horizontal surfaces on the glacier tongue and periglacial area (Seier et al., 2017),
414 unless the camera is tilted to an off-nadir viewpoint (Dewez et al., 2016; Aicardi et al., 2016). Results
415 obtained from photogrammetry based on terrestrial and UAV platforms can thus be retained quite
416 complementary.

417 In agreement with other studies of vertical rock slopes (e.g. Abellan et al., 2014), we found that the
418 TLS point cloud was affected by occlusions (see e.g. location 2 in Fig. 6). Data acquisition with this
419 platform is in general difficult in regions that are subparallel to the laser beams and in the presence of
420 wet surfaces. Its main disadvantage compared to photogrammetry is however the complexity of
421 instrument transport and setup. In terms of logistics, up to five people were involved in the
422 transportation of the TLS instruments (laser scanner, theodolite, at least two topographic tripods and
423 poles, electric generator and ancillary accessories) while 2 people were required for UAV and close-
424 range photogrammetric surveys. Meteorological conditions and the limited access to unstable areas
425 close to the glacier terminus also prevented the acquisition of TLS data from other viewpoints as done
426 with photogrammetry. Finally, TLS instruments are much more expensive at 70000-100000€ compared
427 to UAVs (3500€ for our platform) and DSLR (Digital Single-Lens Reflex) cameras used in
428 photogrammetry, in the range 500-3500€.

429 In this study, the uncertainty of the 2016 UAV dataset (40.5 cm RMSE on GCPs and 21.1-37.7 cm
430 RMSE when compared against TLS) was slightly higher than previously reported in high mountain
431 glacial environments (Immerzeel et al., 2014; Gindraux et al., 2017; Seier et al., 2017). Contributing
432 factors might include the sub-optimal distribution and density of GCPs (Gindraux et al., 2017), the
433 delay between the UAV surveys as well as between UAV and other surveys and the lack of
434 coincidence between GCP placement and the UAV flights. This means the UAV photogrammetric
435 reconstruction was affected by ice ablation and glacier flow, which on Forni Glacier range between 3-5
436 cm day⁻¹ (Senese et al., 2012) and 1-4 cm day⁻¹, respectively (Urbini et al., 2017). We thus expect a
437 combined 3-day uncertainty on the 2016 UAV dataset between 10 and 20 cm, and lower on GCPs
438 considering reduced ablation owing to their placement on boulders. A further contribution to the error
439 budget of GCPs might stem from the intrinsic precision of GNSS/theodolite measurements and image

440 resolution. The comparison between close-range photogrammetry and TLS, was less affected by
441 glacier change as data were collected one day apart and the RMSE of 6-10.6 cm is in line with previous
442 findings by Kaufmann and Landstaedter (2008). To improve the accuracy of UAV photogrammetric
443 blocks, a better distribution of GCPs or switching to an RTK system should be considered, while close-
444 range photogrammetry could benefit from measuring a part of the photo-stations as proposed in Forlani
445 et al. (2014), instead of placing GCPs on the glacier surface.

446 The uncertainty in UAV photogrammetric reconstruction also factored in the relatively high standard
447 deviation still present after the coregistration between DEMs in areas outside the glacier (2.22 m
448 between 2014 and 2016). Another important factor here is the morphology of the coregistration area,
449 i.e. the outwash plain, still subject to changes owing to the inflow of glacier meltwater and sediment
450 reworking. The final accuracy of our UAV photogrammetric products was nevertheless adequate to
451 investigate ice thickness changes over 2 years, while the integration with close-range photogrammetry
452 was required to investigate hazards related to the collapse of the glacier terminus.

453 We conducted UAV surveys under different meteorological scenarios, and obtained adequate results
454 with early-morning operations with 0/8 cloud cover and midday flights with 8/8 cloud cover. Both
455 scenarios can provide diffuse light conditions allowing to collect pictures suitable for photogrammetric
456 processing, but camera settings need to be carefully adjusted beforehand (O'Connor et al., 2017). If
457 early morning flights are not feasible in the study area for logistical reasons or when surveying east-
458 exposed glaciers, the latter scenario should be considered.

459 In our pilot study, we covered part of the Forni glacier tongue, and only investigated hazards related to
460 the glacier collapse. Our maps can help identify safer paths where mountaineers and skiers can visit the
461 glacier and reach the most important summits. However, the increase in collapse structures owing to

462 climate change requires multi-temporal monitoring. A comprehensive risk assessment should also
463 cover the entire glacier, to investigate the probability of serac detachment and provide an estimate of
464 the glacier mass balance with the geodetic method. While our integrated approach using a multicopter
465 and terrestrial photogrammetry should be preferred to investigate small individual ice bodies, fixed-
466 wing UAVs, ideally equipped with an RTK system and ability to tilt the camera off-nadir, might be the
467 platform of choice to cover large distances (see e.g. Ryan et al., 2017), potentially reducing the number
468 of flights and solving issues with GCP placement. Such platforms could help collect sufficient data for
469 hazard management strategies up to the basin scale in Stelvio National Park and other sectors of the
470 Italian Alps, eventually replacing aerial LiDAR surveys. Cost analyses (Matese et al., 2015) should
471 also be performed to evaluate the benefits of improved spatial resolution and DEM accuracy of UAVs
472 compared to aerial and satellite surveys and choose the best approach for individual cases.

473 7 Conclusions

474 In our study, we compared point clouds generated from UAV photogrammetry, close-range
475 photogrammetry and TLS to assess their quality and evaluate the potential in mapping and describing
476 glacier hazards such as ring faults and normal faults, by carrying out a specific campaign in summer
477 2016. In addition, we employed orthophotos and point clouds from a UAV survey conducted in 2014 to
478 analyze the evolution of glacier hazards and a DEM from an aerial photogrammetric survey conducted
479 in 2007 to investigate glacier thickness changes between 2014 and 2016. The main findings of our
480 study include:

- 481 • UAVs and terrestrial photogrammetric surveys provide reliable performances in glacial
482 environments, outperform TLS in terms of logistics and costs, and are more flexible in relation
483 to meteorological conditions.

- UAV and terrestrial photogrammetric blocks can be easily integrated providing more information than individual techniques to help identify glacier hazards.
- UAV-based DEMs can be employed to estimate thickness changes but improvements are necessary in terms of area covered and accuracy **to calculate the geodetic mass balance** of large glaciers.
- The Forni Glacier is rapidly collapsing with an increase in ring faults size, providing evidence of climate change in the region.
- The glacier thinning rate increased owing to collapses to $5.20 \pm 1.11 \text{ ma}^{-1}$ between 2014 and 2016.

The maps produced from the combined analysis of UAV and terrestrial photogrammetric **point clouds** can be made available through GIS web portals of Stelvio National Park or Lombardy region (<http://www.geoportale.regione.lombardia.it/>). A permanent monitoring programme should be setup to help manage risk in the area, issuing warnings and assisting mountain guides in changing hiking and ski routes as needed. The analysis of glacier thickness changes suggests a feedback mechanism which should be further analysed, with higher thinning rates leading to increased occurrence of collapses, **with additional release of meltwater**. Glacier downwasting is also of relevance for risk management in the protected area, providing valuable data to assess the increased chance of rockfalls and to improve forecasts of glacier meltwater production.

While our test was conducted on one of the largest glaciers in the Italian Alps, the integrated photogrammetric approach is easily transferrable to similar sized and much smaller glaciers, where it would be able to provide a comprehensive assessment of hazards and **mass balance** and become useful in decision support systems for natural hazard management. In larger regions, UAVs hold the potential

506 to become the platform of choice but their performances and cost-effectiveness compared to aerial and
507 satellite surveys need to be further evaluated.

508 **Competing interests**

509 The authors declare that they have no conflict of interest.

510 **Acknowledgements**

511 This study was funded by DARAS, the department for autonomies and regional affairs of the
512 presidency of the council of the Italian government. The authors acknowledge the central scientific
513 committee of CAI (Club Alpino Italiano – Italian Alpine Club) and Levissima San Pellegrino S.P.A.
514 for funding the UAV quadcopter. The authors also thank Stelvio Park Authority for the logistic support
515 and for permitting the UAV surveys and IIT Regione Lombardia for the provision of the 2007 DEM.
516 Acknowledgements also go to the GICARUS lab of Politecnico Milano at Lecco Campus for providing
517 the survey equipment. Finally, the authors would also like to thank Tullio Feifer, Livio Piatta, and
518 Andrea Grossoni for their help during field operations.

519 **References**

- 520 Abellán, A., Oppikofer, T., Jaboyedoff, M., Rosser, N. J., Lim, M. and Lato, M. J.: Terrestrial laser
521 scanning of rock slope instabilities. *Earth Surface Processes and Landforms*, 39, 80–97, 2014,
522 doi:10.1002/esp.3493.
- 523 Aicardi, I., Chiabrando, F., Grasso, N., Lingua, A.M., Noardo, F. and Spanò, A.: UAV photogrammetry
524 with oblique images: first analysis on data acquisition and processing, *International Archives of the*
525 *Photogrammetry, Remote Sensing and Spatial Information Sciences*, XXIII ISPRS Congress, Prague,
526 Czech Republic, 12–19 July 2016, 41-B1, 835-842, 2016, doi: 10.5194/isprs-archives-XLI-B1-835-
527 2016.
- 528 Azzoni, R.S., Fugazza, D., Zennaro, M., Zucali, M., D’Agata, C., Maragno, D., Cernuschi, M.,
529 Smiraglia, C. and Diolaiuti, G.A.: Recent structural evolution of Forni Glacier tongue (Ortles-Cevedale
530 Group, Central Italian Alps), submitted to *Journal of Maps*.
- 531 Berthier, E., Arnaud, Y., Kumar, R., Ahmad, S., Wagnon, P. and Chevallier, P.: Remote sensing
532 estimates of glacier mass balances in the Himachal Pradesh (Western Himalaya, India), *Remote*
533 *Sensing of Environment*, 108, 327-338, 2007, doi: 10.1016/j.rse.2006.11.017.

- 534 Berthier, E., Cabot, V., Vincent, C. and Six, D.: Decadal Region-Wide and Glacier-Wide Mass
535 Balances Derived from Multi-Temporal ASTER Satellite Digital Elevation Models. Validation over the
536 Mont-Blanc Area, *Frontiers in Earth Science*, 4, 63, 2016, doi: 10.3389/feart.2016.00063.
- 537 Bhardwaj, A., Sam, L., Akanksha, Martin-Torres, F.J. and Kumar, R.: UAVs as remote sensing
538 platform in glaciology: Present applications and future prospects, *Remote Sensing of Environment*,
539 175, 196-204, 2016, doi: 10.1016/j.rse.2015.12.029.
- 540 Blasone, G., Cavalli, M. and Cazorzi, F.: Debris-Flow Monitoring and Geomorphic Change Detection
541 Combining Laser Scanning and Fast Photogrammetric Surveys in the Moscardo Catchment (Eastern
542 Italian Alps), in: Lollino, G., Arattano, M., Rinaldi, M., Giustolisi, O., Marechal, J.C. and Grant, G.
543 (eds) *Engineering Geology for Society and Territory*, 3, Springer, Cham, 51-54, 2015, doi:
544 10.1007/978-3-319-09054-2_10.
- 545 Carey, M., McDowell, G., Huggel, C., Jackson, M., Portocarrero, C., Reynolds, J.M. and Vicuña, L.:
546 Integrated approaches to adaptation and disaster risk reduction in dynamic sociocryospheric systems,
547 in: Haeberli, W. and Whiteman, C. (Eds.), *Snow and Ice-related Hazards, Risks and Disasters*, Elsevier,
548 219-261, 2014, doi: 10.1016/B978-0-12-394849-6.00008-1.
- 549 Clague, J.: Glacier Hazards, in: Bobrowski, P. (Ed.), *Encyclopedia of Natural Hazards*, Springer, 400-
550 405, 2013, doi: 10.1007/978-1-4020-4399-4_156.
- 551 Chiarle, M., Iannotti, S., Mortara, G. and Deline, P.: Recent debris flow occurrences associated with
552 glaciers in the Alps, *Global and Planetary Change*, 56, 123-136, 2007, doi:
553 10.1016/j.gloplacha.2006.07.003.
- 554 Colomina, I. and Molina, P.: Unmanned aerial systems for photogrammetry and remote sensing: A
555 review, *ISPRS Journal of Photogrammetry and Remote Sensing*, 92, 79-97, 2014, doi:
556 10.1016/j.isprsjprs.2014.02.013.
- 557 D'Agata, C., Bocchiola, D., Maragno, D., Smiraglia, C. and Diolaiuti, G.A.: Glacier shrinkage driven
558 by climate change during half a century (1954–2007) in the Ortles-Cevedale group (Stelvio National
559 Park, Lombardy, Italian Alps), *Theoretical and Applied Climatology*, 116, 169-190, 2014, doi:
560 10.1007/s00704-013-0938-5.
- 561 Dewez, T.J.B., Leroux, J. and Morelli, S.: Cliff collapse hazard from repeated multicopter UAV
562 acquisitions: return on experience, *The International Archives of the Photogrammetry, Remote Sensing
563 and Spatial Information Sciences*, XXIII ISPRS Congress, Prague, Czech Republic, 12–19 July 2016,
564 41-B5, 805-811, 2016, doi: 10.5194/isprs-archives-XLI-B5-805-2016
- 565 Diolaiuti, G.A. and Smiraglia, C.: Changing glaciers in a changing climate: how vanishing
566 geomorphosites have been driving deep changes in mountain landscapes and environments,
567 *Géomorphologie : Relief, Processus, Environnement*, 2, 131-152, 2010, doi:
568 10.4000/geomorphologie.7882.
- 569 Diolaiuti, G.A., Bocchiola, D., D'Agata, C. and Smiraglia, C.: Evidence of climate change impact upon
570 glaciers' recession within the Italian Alps, *Theoretical and Applied Climatology*, 109, 429-445, 2012, doi:
571 10.1007/s00704-012-0589-y

- 572 Eltner, A., Kaiser, A., Castillo, C., Rock, G., Neugirg, F. and Abellán, A.: Image-based surface
573 reconstruction in geomorphometry – merits, limits and developments. *Earth Surface Dynamics*, 4, 359-
574 389, 2016, doi: 10.5194/esurf-4-359-2016.
- 575 Fioletti, M., Bonetti, M., Smiraglia, C., Diolaiuti, G.A., Breganze, C., dal Toso, M. and Facco, L.:
576 Indagini radar per lo studio delle caratteristiche endoglaciali del ghiacciaio dei Forni in alta Valtellina,
577 *Neve e Valanghe*, 87, 40-45, 2016
- 578 Fischer, M., Huss, M., Barboux, C. and Hoelzle, M.: The new Swiss Glacier Inventory SGI2010:
579 relevance of using high-resolution source data in areas dominated by very small glaciers, *Arctic, Antarctic*
580 *and Alpine Research*, 46,933-945, 2014, doi: 10.1657/1938-4246-46.4.933.
- 581 Fischer, M., Huss, M. and Hoelzle, M.: Surface elevation and mass changes of all Swiss glaciers 1980–
582 2010, *The Cryosphere*, 9, 525-540, 2015, doi: 10.5194/tc-9-525-2015
- 583 Forlani, G., Pinto, L., Roncella, R. and Pagliari, D.: Terrestrial photogrammetry without ground control
584 points, *Earth Science Informatics*, 7, 71-81, 2014, doi: 10.1007/s12145-013-0127-1.
- 585 Fugazza, D., Senese, A., Azzoni, R.S., Smiraglia, C., Cernuschi, M., Severi, D. and Diolaiuti, G.A.:
586 High-resolution mapping of glacier surface features. The UAV survey of the Forni glacier (Stelvio
587 national park, Italy), *Geografia Fisica e Dinamica Quaternaria*, 38, 25-33, 2015, doi:
588 10.4461/GFDQ.2015.38.03.
- 589 Furukawa, Y. and Ponce, J.: Accurate Camera Calibration from Multi-View Stereo and Bundle
590 Adjustment, *International Journal of Computer Vision*, 84, 257–268, 2009, doi: 10.1007/s11263-009-
591 0232-2.
- 592 Garavaglia, V., Diolaiuti, G.A., Smiraglia, C., Pasquale, V. and Pelfini, M.: Evaluating Tourist
593 Perception of Environmental Changes as a Contribution to Managing Natural Resources in Glacierized
594 areas: A Case Study of the Forni Glacier (Stelvio National Park, Italian Alps), *Environmental*
595 *Management*, 50, 1125-1138, 2012, doi: 10.1007/s00267-012-9948-9.
- 596 Gagliardini, O., Gillet-Chaulet, F., Durand, G., Vincent, C. and Duval, P.: Estimating the risk of glacier
597 cavity collapse during artificial drainage: The case of Tête Rousse Glacier, *Geophysical Research*
598 *Letters*, 38, L10505, 2011, doi:10.1029/2011GL047536.
- 599 Gardent, M., Rabatel, A., Dedieu, J.-P., Deline, P.: Multitemporal glacier inventory of the French Alps
600 from the late 1960s to the late 2000s, *Global and Planetary Change*, 120, 24-37, 2014. doi:
601 10.1016/j.gloplacha.2014.05.004.
- 602 Gindraux, S., Boesch, R. and Farinotti, D.: Accuracy Assessment of Digital Surface Models from
603 Unmanned Aerial Vehicles’ Imagery on Glaciers, *Remote sensing*, 9, 186, 2-15, 2017,
604 doi:10.3390/rs9020186.
- 605 Gobiet, A., Kotlarski, S., Beniston, M., Heinrich, G., Rajczak, J., Stoffel, M.: 21st century climate
606 change in the European Alps—A review, *Science of The Total Environment*, 493, 1138-1151, 2014,
607 doi: 10.1016/j.scitotenv.2013.07.050.

608 Harris, C., Arenson, L.U., Christiansen, H.H., Etzelmueller, B., Frauenfelder, R., Gruber, S., Haeberli,
 609 W., Hauck, C., Hoelzle, M., Humlum, O., Isaksen, K., Kaab, A., Kern-Luetschg, M., Lehning, M.,
 610 Matsuoka, N., Murton, J.B., Noetzli, J., Phillips, M., Ross, N., Seppaelae, M., Springman, S.M. and
 611 Vonder Muehll, D.: Permafrost and climate in Europe: Monitoring and modelling thermal,
 612 geomorphological and geotechnical responses, *Earth-Science Reviews*, 92, 117-171, 2009, doi:
 613 10.1016/j.earscirev.2008.12.002.

614 Hoffmann-Wellenhof, B., Lichtenegger, H. and Wasle, E.: *GNSS – GPS, GLONASS, Galileo & more*,
 615 Springer, 2008, doi: 10.1007/978-3-211-73017-1.

616 Howat, I.M., Smith, B.E., Joughin, I. and Scambos, T.A.: Rates of southeast Greenland ice volume loss
 617 from combined ICESat and ASTER observations, *Geophysical Research Letters*, 35, L17505, 2008,
 618 doi:10.1029/2008GL034496.

619 Immerzeel, W.W., Kraaijenbrink, P.D.A., Shea, J.M., Shrestha, A.B., Pellicciotti, F., Bierkens, M.F.P.
 620 and de Jong, S.M.: High-resolution monitoring of Himalayan glacier dynamics using unmanned aerial
 621 vehicles, *Remote Sensing of Environment*, 150,93-103, 2014, doi: 10.1016/j.rse.2014.04.025.

622 Jokinen, O. and Geist T.: Accuracy aspects in topographical change detection of glacier surface, in:
 623 *Remote sensing of glaciers*, CRC Press/Balkema, Leiden, the Netherlands, 269-283, 2010, doi:
 624 10.1201/b10155-15.

625 Kaab, A., Huggel, C., Fischer, L., Guex, S. Paul, F., Roer., I., Salzmann, N., Schlaefli, S., Schmutz,
 626 K., Schneider, D., Strozzi, T. and Weidmann, Y.: Remote sensing of glacier- and permafrost-related
 627 hazards in high mountains: an overview, *Natural Hazards and Earth System Sciences*, 5, 527–554,
 628 2005a, doi: 10.5194/nhess-5-527-2005.

629 Kaab, A., Reynolds, J.M. and Haeberli, W.: Glacier and Permafrost hazards in high mountains, in:
 630 Huber U.M., Bugmann H.K.M., Reasoner M.A. (eds) *Global Change and Mountain Regions. Advances*
 631 *in Global Change Research*, Springer, Dordrecht, 225-234, 2005b, doi: 10.1007/1-4020-3508-X_23.

632 Kaufmann, V. and Ladstädter, R.: Application of terrestrial photogrammetry for glacier monitoring in
 633 Alpine environments, *International Archives of the Photogrammetry, Remote Sensing and Spatial*
 634 *Information Sciences*, Beijing, China, 37-B8, 813-818, 2008.

635 Kaufmann, V. and Seier, G.: Long-term monitoring of glacier change at Gössnitzkees (Austria) using
 636 terrestrial photogrammetry, *The International Archives of the Photogrammetry, Remote Sensing and*
 637 *Spatial Information Sciences*, XXIII ISPRS Congress, Prague, Czech Republic, 12-19 July 2016, 41-
 638 B8, 495-502, 2016, doi: 10.5194/isprs-archives-XLI-B8-495-2016

639 Keiler, M., Knight, J. and Harrison, S.: Climate change and geomorphological hazards in the eastern
 640 European Alps, *Philosophical Transactions of The Royal Society A*, 368, 2461–2479, 2010, doi:
 641 10.1098/rsta.2010.0047.

642 Kellerer-Pirklbauer, A., Bauer, A. and Proske, H.: Terrestrial laser scanning for glacier monitoring:
 643 Glaciation changes of the Gößnitzkees glacier (Schober group, Austria) between 2000 and 2004, 3rd
 644 Symposium of the Hohe Tauern National Park for research in protected areas, castle of Kaprun, Austria,
 645 15-17 September 2005, 97-106, 2005.

646 Lague, D., Brodu, N., Leroux, J.: Accurate 3D comparison of complex topography with terrestrial laser
647 scanner: application to the Rangitikei canyon (N-Z). *Journal of Photogrammetry and Remote Sensing*,
648 82, 10–26, 2013, doi:10.1016/j.isprsjprs.2013.04.009.

649 Matese, A., Toscano, P., Di Gennaro, S.F., Genesio, L., Vaccari, F.P., Primicerio, J., Belli, C., Zaldei,
650 A., Bianconi, R., Gioli, B.: Intercomparison of UAV, Aircraft and Satellite Remote Sensing Platforms
651 for Precision Viticulture, *Remote Sensing*, 7, 2971-2990, 2015, doi:10.3390/rs70302971.

652 Mugnier, C.J.: Grids & Datum. Italian Republic. *Photogrammetric Engineering and Remote Sensing*,
653 71, 889-890, 2005.

654 Nuth, C. and Kaab, A.: Co-registration and bias corrections of satellite elevation data sets for
655 quantifying glacier thickness change, *The Cryosphere*, 5, 271-290, 2011, doi: 10.5194/tc-5-271-2011.

656 Osborne, M.: Mission planner software. Available at: <http://ardupilot.org/planner/>, last access:
657 18/05/2017, 2013.

658 O'Connor, J., Smith, M.J. and James, M.R.: Cameras and settings for aerial surveys in the geosciences:
659 optimising image data, *Progress in Physical Geography*, 41, 1-20, 2017, doi:
660 10.1177/0309133317703092.

661 Palomo, I.: Climate Change Impacts on Ecosystem Services in High Mountain Areas: A Literature
662 Review, *Mountain Research and Development*, 37, 179-187, 2017, doi: 10.1659/MRD-JOURNAL-D-
663 16-00110.1.

664 Piermattei, L., Carturan, L. and Guarnieri, A.: Use of terrestrial photogrammetry based on structure
665 from motion for mass balance estimation of a small glacier in the Italian Alps. *Earth Surface Processes
666 and Landforms*, 40, 1791-1802, 2015, doi: 10.1002/esp.3756.

667 Piermattei, L., Carturan, L., de Blasi, F., Tarolli, P., Dalla Fontana, G., Vettore, A. and Pfeifer, N.:
668 Suitability of ground-based SfM–MVS for monitoring glacial and periglacial processes, *Earth Surface
669 Dynamics*, 4, 325-443, 2016, doi: 10.5194/esurf-4-425-2016.

670 Pomerleau, F., Colas, F., Siegwart, R. and Magnenat, S.: Comparing ICP variants on real world data
671 sets. *Autonomous Robots*, 34, 133–148, 2013, doi: 10.1007/s10514-013-9327-2.

672 Quincey, D.J., Lucas, R.M., Richardson, S.D., Glasser, N.F., Hambrey, N.J. and Reynolds, J.M.:
673 Optical remote sensing techniques in high-mountain environments: application to glacial hazards,
674 *Progress in Physical Geography*, 29, 475-505, 2005, doi: 10.1191/0309133305pp456ra.

675 Riccardi, A., Vassena, G., Scotti, R., Sgrenzaroli, M.: Recent evolution of the punta S.Matteo serac
676 (Ortles-Cevedale Group, Italian Alps), *Geografia Fisica e Dinamica Quaternaria*, 33, 215-219, 2010.

677 Rounce, D.R., Watson, C.S. and McKinney, D.C.: Identification of Hazard and Risk for Glacial Lakes
678 in the Nepal Himalaya Using Satellite Imagery from 2000–2015, *Remote Sensing*, 9, 654, 2017,
679 doi:10.3390/rs9070654.

680 Ryan, J.C., Hubbard, A., Box, J.E., Brough, S., Cameron, K., Cook, J.M., Cooper, M., Doyle, S.H.,
681 Edwards, A., Holt, T., Irvine-Fynn, T., Jones, C., Pitcher, L.H., Rennermalm, A.K., Smith, L.C, Stibal,

682 M. and Snooke, N.: Derivation of High Spatial Resolution Albedo from UAV Digital Imagery:
683 Application over the Greenland Ice Sheet, *Frontiers in Earth Science*, 5, 40, 2017, doi:
684 10.3389/feart.2017.00040.

685 Seier, G., Kellerer-Pirklbauer, A., Wecht, M., Hirschmann, S., Kaufmann, V., Lieb, G.K. and Sulzer,
686 W.: UAS-Based Change Detection of the Glacial and Proglacial Transition Zone at Pasterze Glacier,
687 Austria. *Remote Sensing*, 9, 549, 2017, doi:10.3390/rs9060549.

688 Senese, A., Diolaiuti, G.A., Mihalcea, C. and Smiraglia, C.: Energy and Mass Balance of Forni Glacier
689 (Stelvio National Park, Italian Alps) from a Four-Year Meteorological Data Record, *Arctic, Antarctic
690 and Alpine Research*, 44, 122-134, 2012, doi: 10.1657/1938-4246-44.1.122.

691 Smiraglia, C., Azzoni, R.S., D'Agata, C., Maragno, D., Fugazza, D. and Diolaiuti, G.A.: The evolution
692 of the Italian glaciers from the previous data base to the new Italian inventory. Preliminary
693 considerations and results, *Geogr. Fis. Dinam. Quat.*, 38, 79-87, 2015, doi: 10.4461/GFDQ.2015.38.08.

694 Spetsakis, M. and Aloimonos, J.Y.: A multi-frame approach to visual motion perception, *International
695 Journal of Computer Vision*, 6, 245-255, 1991, doi: 10.1007/BF00115698.

696 Teunissen, P.J.G.: Testing theory. An introduction. Series on Mathematical Geodesy and Positioning,
697 VSSD Delft, The Netherlands, 2009.

698 Urbini, S., Zirizzotti, A., Baskaradas, J.A., Tabacco, I.E., Cafarella, L., Senese, A., Smiraglia, C.,
699 Diolaiuti, G.: Airborne radio echo sounding (RES) measures on alpine glaciers to evaluate ice
700 thickness and bedrock geometry: Preliminary results from pilot tests performed in the ortles-cevedale
701 group (Italian alps), *Annals of Geophysics*, 60, G0226, doi: 10.4401/ag-7122, 2017.

702 Vincent, C., Thibert, E., Harter, M., Soruco, A. and Gilbert, A.: Volume and frequency of ice
703 avalanches from Tacconnaz hanging glacier, French Alps, *Annals of Glaciology*, 56, 17-25, 2015, doi:
704 10.3189/2015AoG70A017.

705 Westoby, M.J., Brasington, J., Glasser, N.F., Hambrey, M.J. and Reynolds, J.M.: Structure-from-
706 Motion' photogrammetry: A low-cost, effective tool for geoscience applications, *Geomorphology*, 179,
707 300-314, 2012, doi: 10.1016/j.geomorph.2012.08.021.

708 Winkler, M., Pfeffer, W.T. and Hanke, K.: Kilimanjaro ice cliff monitoring with close range
709 photogrammetry, *International Archives of the Photogrammetry, Remote Sensing and Spatial
710 Information Sciences*, XXII ISPRS Congress, Melbourne, Australia, 25 August-1 September 2012, 39-
711 B5, 441-446, 2012.

712

713 **Tables**

DEM pair	Elevation differences without co- registration shifts ($\mu_{\Delta H} \pm \sigma_{\Delta H}$) [m]	Co-registration shifts		Elevation differences with co-registration shifts ($\mu_{\Delta H} \pm \sigma_{\Delta H}$) [m]
		X [m]	Y [m]	
2007-2014	1.96±2.60	1.11	-1.11	0.00±1.70
2007-2016	-0.43±3.48	2.44	-1.11	0.00±2.60
2014-2016	-2.92±3.21	-0.20	-1.30	0.00±2.22

714 *Table 1: Statistics of the elevation differences between DEM pairs before and after the application of*
715 *co-registration shifts.*
716

717

Sam ple Win dow	Area (m ²)	number of points in sample windows			Mean and standard deviation of point density [points/m ²]			Number of point above the lower 12.5% percentile		
		UAV photogra mm.	Terrestri al Photogra mm.	TLS	UAV Photogra mm.	Terrestri al Photogra mm.	TLS	UAV Photogra mm.	Terrestri al Photogra mm.	TLS
1	2793	-	1984k	141k	-	1654±63 7	226± 100	-	880	26
2	1806	76k	2175k	130k	109±29	2297±70 8	391± 217	61	881	0
3	495	43k	712k	25k	103±27	1978±60 6	151± 60	49	766	31
4	672	62k	557k	33k	108±22	1384±53 0	141± 69	62	324	2
5	3960	406k	810k	-	141±22	485±227	-	97	31	-

718

719

720

721

722

Table 2: Area and number of points in each sample window on the Forni Glacier terminus, mean and standard deviation of local point density and number of points above the lower 12.5% percentile in each window.

723

Sample Window		Means and Std. Dev.s of M3C2 distances [cm]			RMSE of M3C2 distances [cm]		
	Ref.	TLS	TLS	UAV Photogramm .	TLS	TLS	UAV Photogramm m.
	Slave	Terrestrial Photogramm .	UAV Photogramm .	Terrestrial Photogramm .	Terrestrial Photogramm m.	UAV Photogramm .	Terrestrial Photogramm m.
1		4.5±7.4	-	-	8.7	-	-
2		-1.1±10.5	14.8±34.7	-14.5±26.7	10.6	37.7	30.4
3		8.4±4.1	14.7±15.1	-8.5±18.9	9.4	21.1	20.7
4		2.8±5.3	9.4±22.2	-2.3±24.9	6.0	24.0	25.0
5		-	-	-8.5±25.3	-	-	26.7

724

725

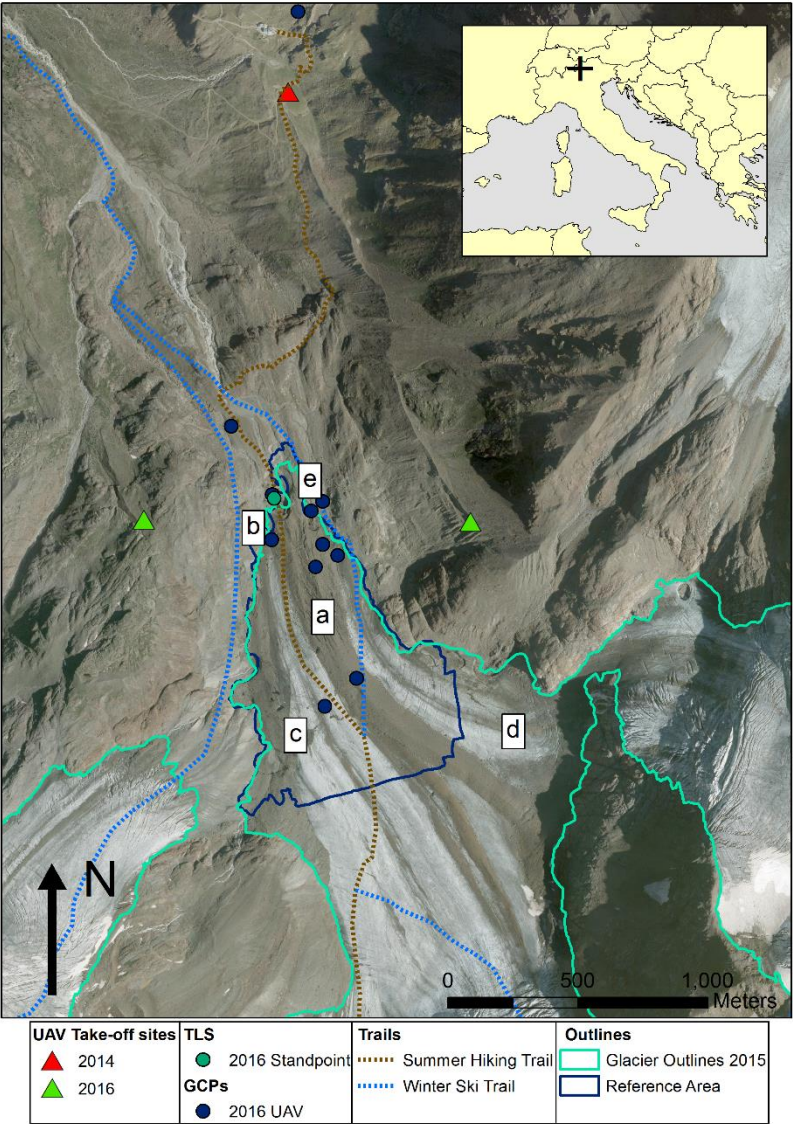
726

Table 3: Statistics on distances between point

727 clouds computed on the basis of M3C2 algorithm.

DEM pair	Mean thickness change [m]	Mean thinning rates [ma ⁻¹]	Volume Change [10 ⁶ m ³]
2007-2014	-31.91 ± 1.70	-4.55 ± 0.24	-10.00 ± 0.12
2007-2016	-42.86 ± 2.60	-4.76 ± 0.29	-13.46 ± 0.14
2014-2016	-10.41 ± 2.22	-5.20 ± 1.11	-3.29 ± 0.05

728 Table 4: Average ice thickness change, thinning rates and volume loss from DEM differencing over a
729 common reference area of 0.32 km² for all DEM pairs. Uncertainty of thickness change expressed as
730 1σ of residual elevation differences over stable areas after DEM co-registration.
731



734
735 *Figure 1: the tongue of Forni Glacier. The map shows the location of take-off/landing sites for*
736 *the 2014 and 2016 UAV surveys (in 2016 two different landing sites were used), standpoint of*
737 *TLS survey, GCPs used in the UAV photogrammetry surveys and trails crossing the glaciers.*
738 *Letters a-e identify the location of features described in Fig.2. Base map from 2015 courtesy of*
739 *IIT Regione Lombardia WMS Service. Trails from Kompass online cartography at*
740 *<https://www.kompass-italia.it/info/mappa-online/>.*

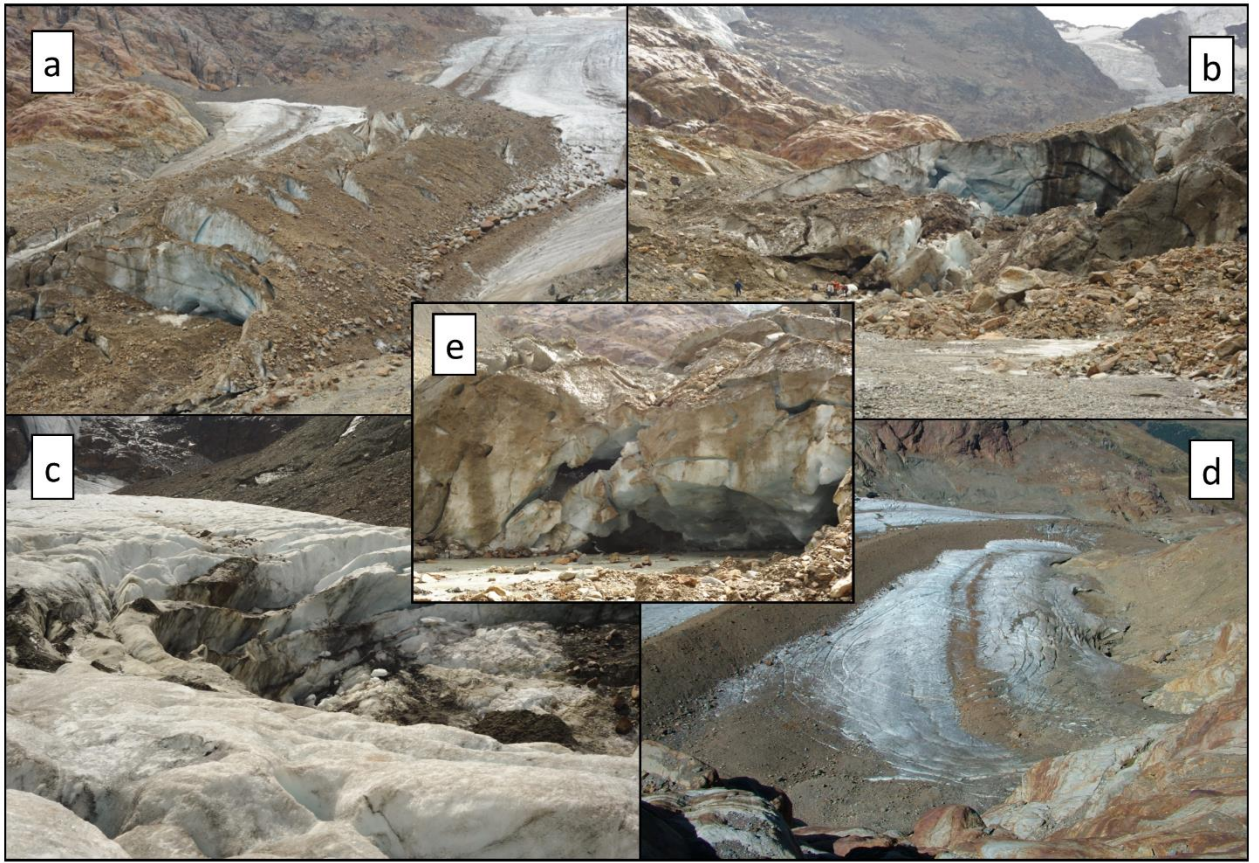


Figure 2: Collapsing areas on the tongue of Forni Glacier. (a) Faults cutting across the eastern medial moraine; (b) glacier terminus; (c) Near-circular collapsed area on the central tongue; (d) Large ring fault on the eastern tongue at the base of the icefall. Photo courtesy of G.Cola; (e) Close-up of a vertical ice cliff at the glacier terminus. The location of features is reported in Fig.1



Aircraft type	Swinglet CAM, Commercial platform
Digital Camera	Canon Ixus 127 HS
Camera technical features	16 Megapixel, focal length 4.3 mm
GNSS antenna	GPS only
Weight (incl. payload)	0.50 Kg
Battery time	30 minutes

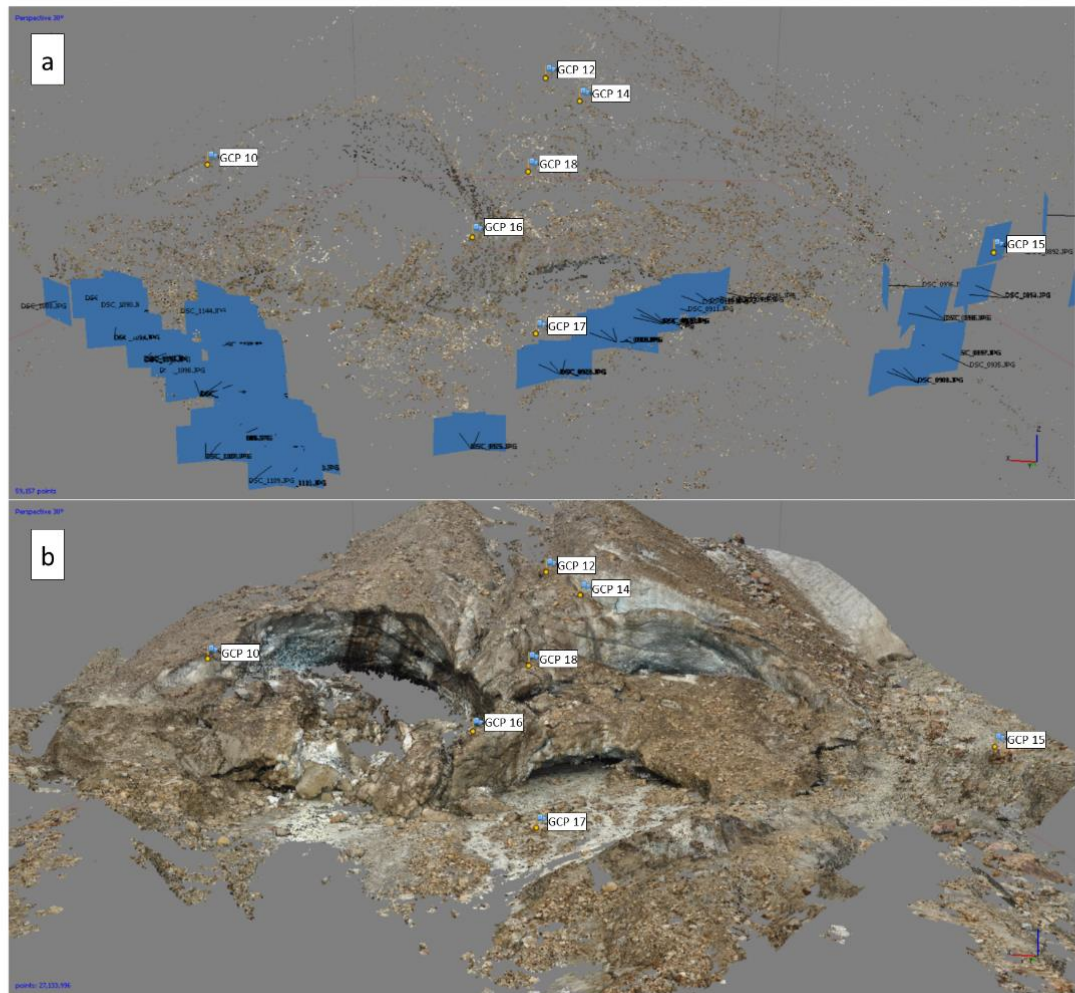


Aircraft type	Customized, with Tarot frame 650 size, VR Brain 5.2 Autopilot & APM Arducopter 3.2.1 Firmware
Digital camera	Canon Powershot ELPH 320 HS
Camera technical features	16 Megapixel, focal length 4.3 mm
GNSS antenna	GPS+GLONASS (Galileo compatible)
Weight (incl. payload)	2.75 Kg
Battery time	20-25 minutes

749

750 *Figure 3: The UAVs used in surveys of the Forni Glacier and their characteristics. (a) The*
 751 *SwingletCam fixed-wing aircraft employed in 2014, at its take off site by Lake Rosole; (b) The*
 752 *customized quadcopter used in 2016 in the lab.*

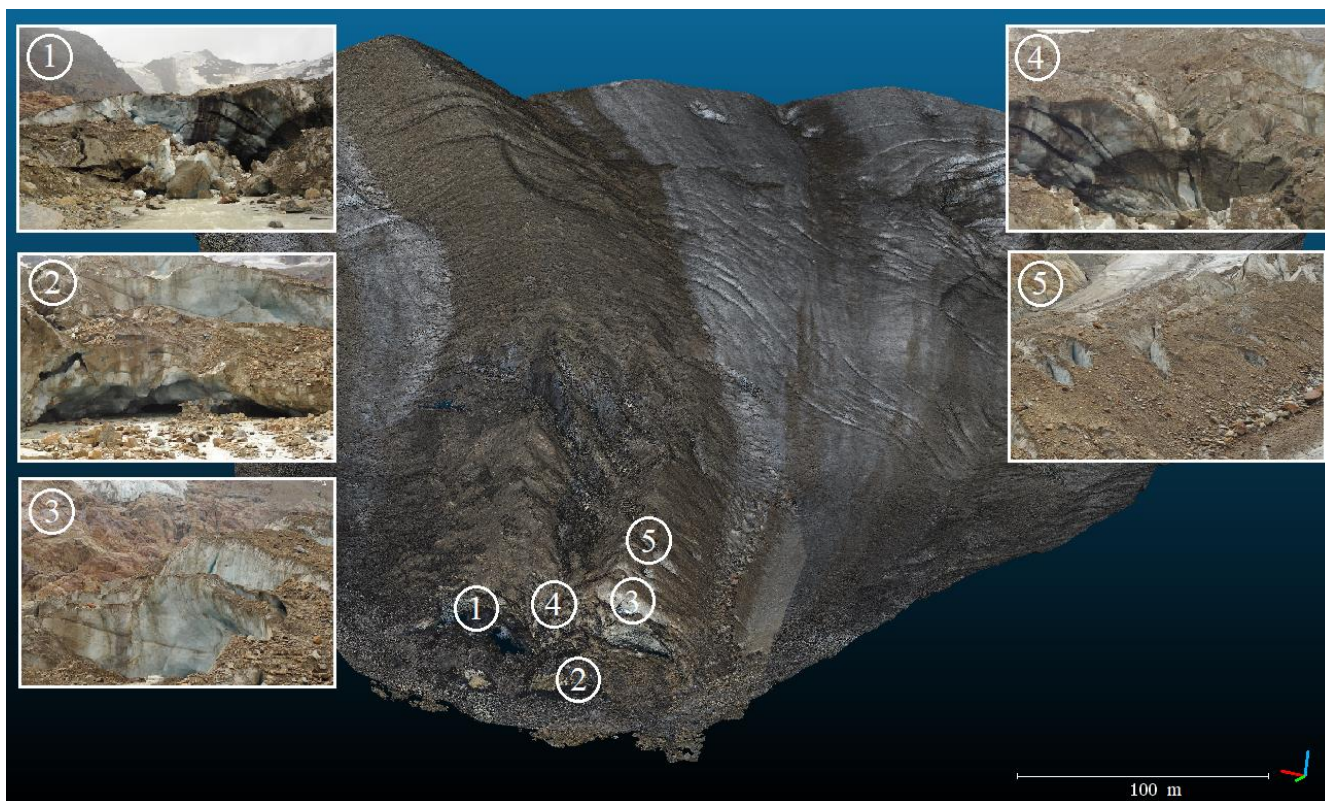
753



754

755 *Figure 4: 3D reconstruction of the glacier terminus from the terrestrial photogrammetric survey of*
 756 *2016 : (a) locations of camera stations in front of the glacier and 3D coordinates of tie points extracted*
 757 *during SfM for image orientation; (b) point cloud of the glacier terminus with positions of GCPs.*

758



759

760 *Figure 5: Location of different glacier features or hazard-prone areas on the tongue of Forni glacier*
 761 *were the point cloud comparison was performed. The background image is the merged point cloud*
 762 *generated from the 2016 UAV and terrestrial photogrammetry survey.*

763

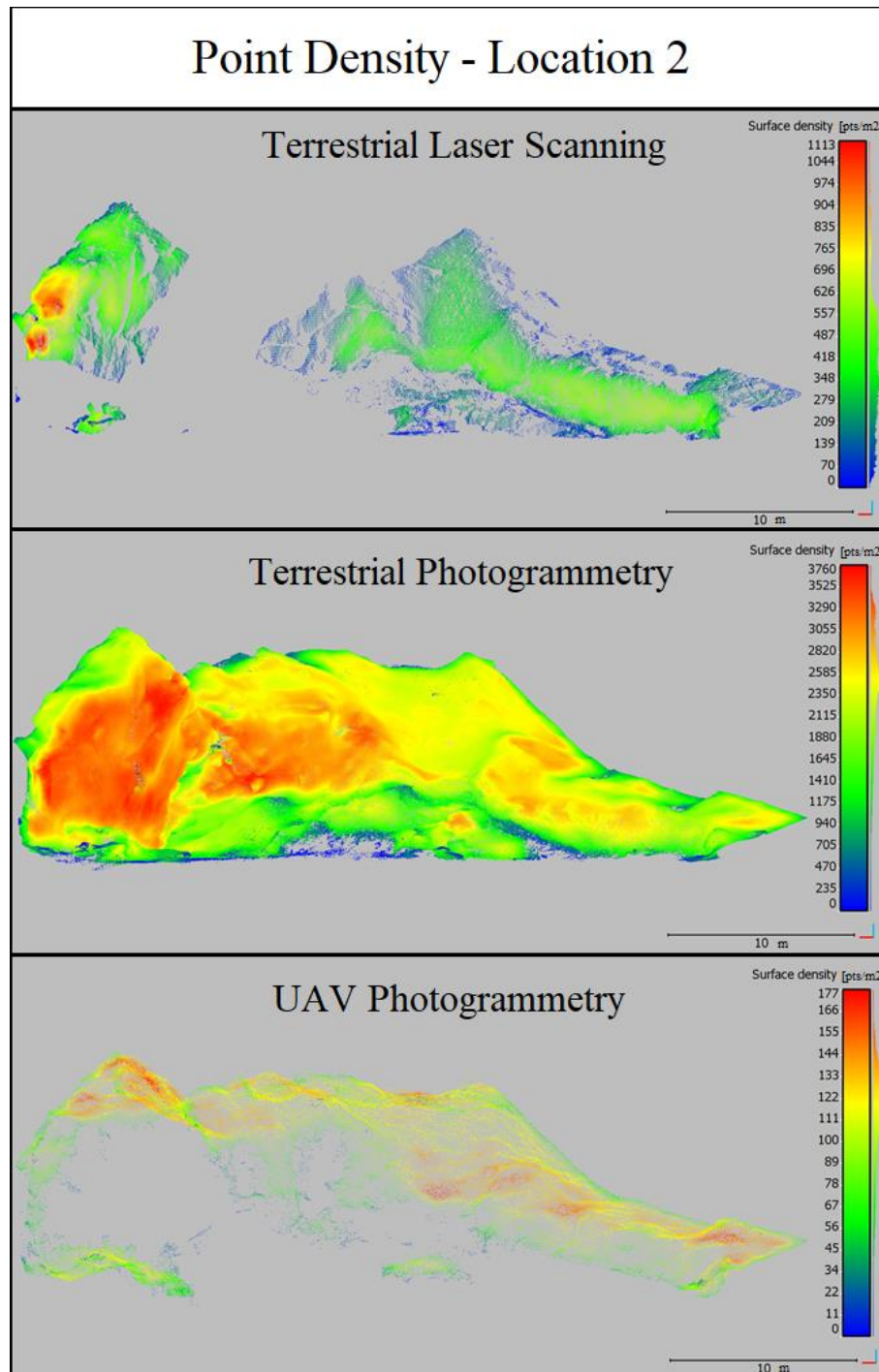
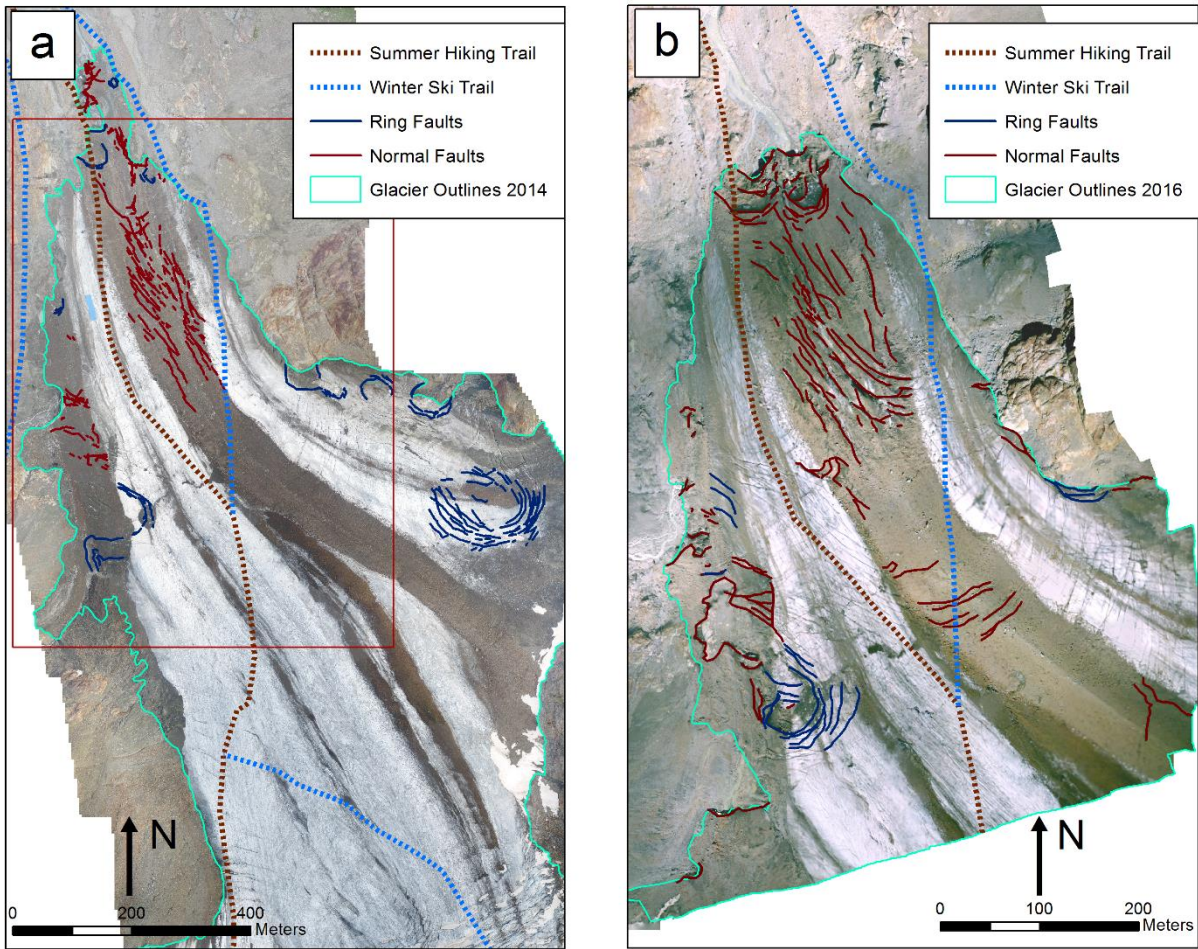


Figure 6: Maps of point density in sample location 2.



767

768 *Figure 7: location of collapse structures, i.e. normal faults and ring faults and trails crossing the Forni*

769 *Glacier (a) 2014, with 2014 UAV ortophoto as basemap. The red box marks the area surveyed in 2016.*

770 *(b) 2016, with 2016 UAV orthophoto as basemap. Trails from Kompass online cartography at*

771 *<https://www.kompass-italia.it/info/mappa-online/>.*

772

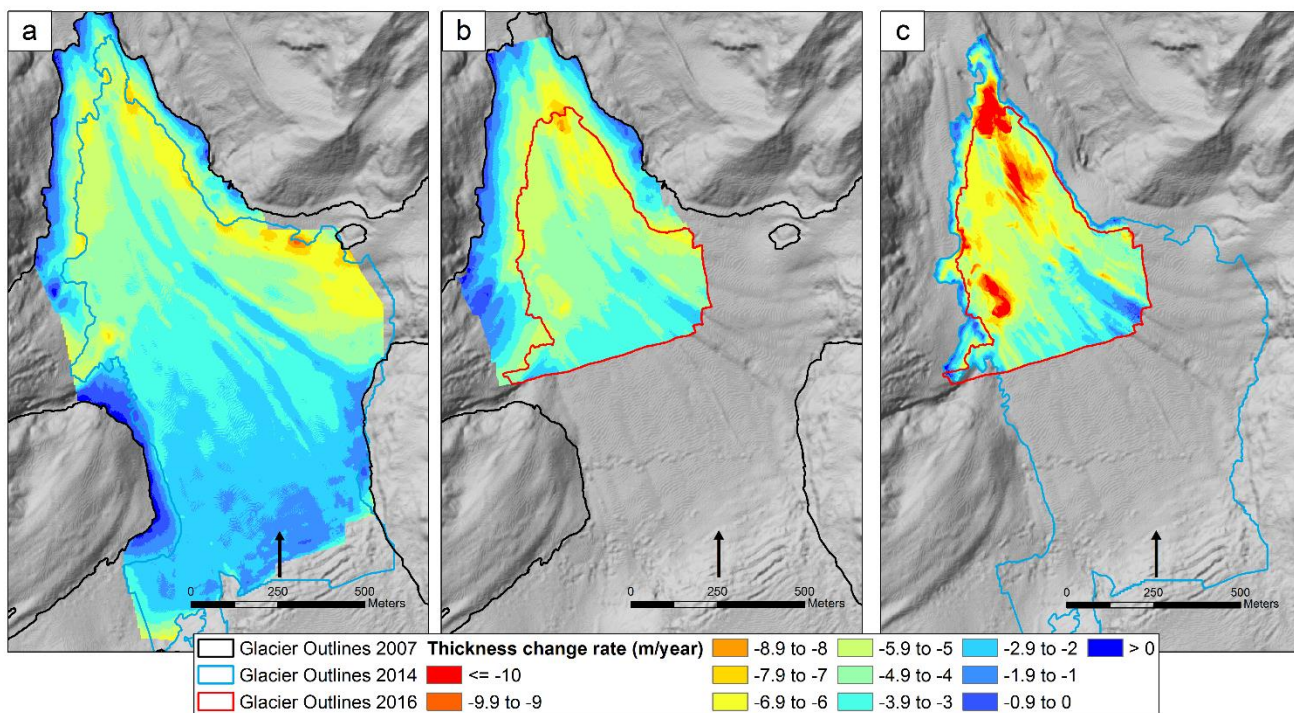


Figure 8: Ice thickness change rates from DEM differencing over (a) 2007-2014; (b) 2007-2016; (c) 2014-2016. Glacier outlines from 2014 and 2016 are limited to the area surveyed during the UAV campaigns. Base map from hillshading of 2007 DEM.